Published in final edited form as:

Immunity. 2017 June 20; 46(6): 1018–1029.e7. doi:10.1016/j.immuni.2017.06.002.

Human leukocyte antigen F (HLA-F) presents peptides and regulates immunity through interactions with NK-cell receptors

Charles L. Dulberger[1], **Curtis P. McMurtrey**[2], **Angelique Hölzemer**[3,4,5], **Karlynn E. Neu**[6], **Victor Liu**[1], **Adriana M. Steinbach**[1], **Wilfredo F. Garcia-Beltran**[7], **Michael Sulak**[8], **Bana Jabri**[9], **Vincent J. Lynch**[8], **Marcus Altfeld**[3], **William H. Hildebrand**[2], and **Erin J. Adams**[1]

[1]Department of Biochemistry and Molecular Biology, The University of Chicago, Chicago, IL 60637, USA

[2]Department of Microbiology and Immunology, The University of Oklahoma Health Sciences Center, Oklahoma City, OK 73104, USA

[3]Heinrich Pette Institute, Leibniz Institute for Experimental Virology, Hamburg, 20251 Germany

[4]First Department of Internal Medicine, Infectious Disease Unit, University Medical Center Hamburg-Eppendorf, 20246 Germany

[5]German Center for Infection Research (DZIF), Hamburg, 20246 Germany

[6]Committee on Immunology, University of Chicago, Chicago, IL 60637, USA

[7]Ragon Institute of MGH, MIT, and Harvard, Cambridge, MA 02139, USA

[8]Department of Human Genetics, The University of Chicago, Chicago, IL 60637, USA

[9]Committee on Immunology, The University of Chicago, Chicago, IL 60637, USA; Department of Medicine, University of Chicago, Chicago, IL 60637, USA

Summary

Evidence is mounting that the major histocompatibility complex (MHC) molecule HLA-F regulates the immune system in pregnancy, infection, and autoimmunity by signaling through NK-cell receptors (NKRs). We present structural, biochemical and evolutionary analyses

Correspondence/Lead Contact: Erin J. Adams, University of Chicago, Dept of Biochemistry and Molecular Biology, 929 E. 57th St. GCIS W236, Chicago, IL 60637, 773-834-9816, ejadams@uchicago.edu.

Author Contributions

C.L.D. designed and performed protein expression, crystallization, structure determination, tetramer staining experiments, binding studies, CD studies and prepared the manuscript. C.P.M and W.H.H. designed, performed and analyzed peptide elution experiments. A.H., W.F.G-B. and M.A. designed and performed the JRC system. V.J.L., C.L.D. and M.S. performed the evolutionary analysis. K.E.N. assisted in 293T protein expression. V.L. and A.M.S. assisted in protein crystallization. B.J. contributed to experimental design and manuscript preparation. E.J.A. led the investigation and contributed to experiment design, data interpretation, and manuscript preparation.

Accession numbers

The coordinates and structure factors for the HLA-F and HLA-F–LIR1 structures have been deposited in the Protein Data Bank under the accession codes 5IUE and 5KNM, respectively.

demonstrating that HLA-F presents peptides of unconventional length dictated by a newly arisen mutation (R62W) that has produced an open-ended groove accommodating particularly long peptides. Compared to empty HLA-F open conformers (OC), HLA-F tetramers bound with human-derived peptides differentially stained leukocytes suggesting peptide-dependent engagement. Our in vitro studies confirm that NKRs differentiate between peptide-bound and peptide-free HLA-F. The complex structure of peptide-loaded β_2m-HLA-F bound to the inhibitory LIR1 revealed similarities to high-affinity recognition of the viral MHC-I mimic UL18 and a docking strategy that relies on contacts with HLA-F as well as β_2m, thus precluding binding to HLA-F OC. These findings provide a biochemical framework to understand how HLA-F could regulate immunity via interactions with NKRs.

eTOC Blurb

HLA-F can regulate immunity as an empty open conformer but whether or not HLA-F can present peptides is controversial. Dulberger et al. show that HLA-F has recently evolved an open-ended antigen-binding groove that facilitates presentation of uncharacteristically long peptides and recognition of HLA-F by NKRs is tunable by peptide binding.

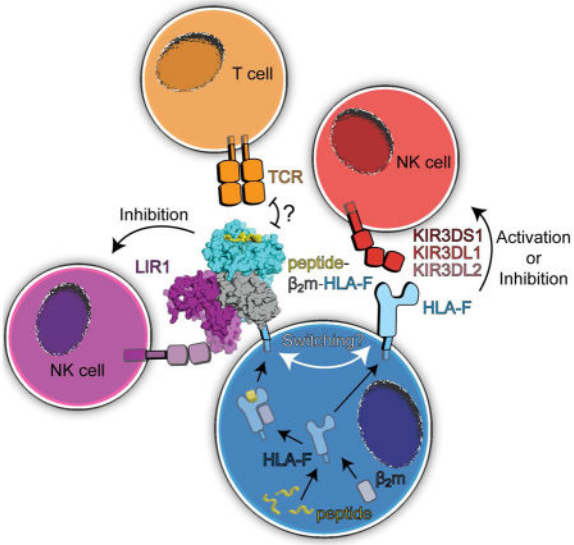

Keywords

HLA-F structure; MHC antigen presentation; MHC-I evolution; NK cell regulation; NK-cell receptor; LIR; KIR

Introduction

Major histocompatibility complex (MHC) molecules allow the immune system to survey the health of virtually every cell in the body. The MHC fold is highly programmable and has been molded throughout evolution to create MHC molecules that are specialized for presentation of lipids, small molecule ligands or peptides. MHC class I (MHC-I) molecules function by binding and displaying self and non-self peptides on the cell surface where they

designate the cell as healthy, infected, or foreign. Leukocytes employ a diverse array of antigen receptors, such as T cell receptors (TCRs) and Natural Killer Cell receptors (NKRs), that perceive the information presented by MHC-I molecules to elicit the appropriate immune response (Adams and Luoma, 2013).

While the MHC-Ia molecules (human leukocyte antigens (HLA) -A, -B and -C) are ubiquitously expressed, the MHC-Ib molecules (HLA-E, -F and -G) are much more specialized in terms of tissue localization, antigen presentation, and function. Because of their limited levels of polymorphism, the repertoire of peptides that MHC-Ib molecules present is greatly reduced (Braud et al., 1997) and they predominantly regulate immunity through TCR-independent interactions. HLA-E preferentially presents peptides derived from the leader sequences of other MHC-I molecules, serving as a sensor of MHC-I expression that protects against lysis via interactions with inhibitory NKRs in the CD94-NKG2 family (Braud et al., 1998). HLA-G is also quite specialized; it primarily presents endogenous peptides at the surface of trophoblasts lining the placenta (Clements et al., 2005), which mostly lacks MHC-Ia expression (Ferreira et al., 2017). At this maternal-fetal interface, HLA-G signals through activating and inhibitory NKRs in the killer-cell immunoglobulin-like receptor (KIR), leukocyte immunoglobulin-like receptor (LIR), and CD94-NKG2 receptor complex families to facilitate maternal tolerance and development of the fetus (Ferreira et al., 2017). Studies have also shown that MHC-Ib molecules can be directly recognized by TCRs on regulatory (Jiang et al., 2010) and cytolytic (Romagnani et al., 2002) T cells.

While HLA-E and HLA-G have been well-characterized functionally and structurally as antigen-presenting molecules, the role that HLA-F plays in regulating the immune system has remained enigmatic until recently. HLA-F has been implicated as a protective molecule in pregnancy (Burrows et al., 2016) and the peripheral nervous system, where HLA-F recognition by the inhibitory KIR3DL2 was shown to prevent motor neuron death in the development of amyotrophic lateral sclerosis (ALS) (Song et al., 2016). It has also been demonstrated that recognition of HLA-F by the activating KIR3DS1 on NK cells elicits an anti-viral response that inhibits HIV-1 replication (Garcia-Beltran et al., 2016). This ability to regulate immunity via KIR3DS1 greatly increases the clinical significance of HLA-F, in light of the broad range of other diseases where KIR3DS1 is implicated (Körner and Altfeld, 2012).

The wide-ranging immunoregulatory capacity of HLA-F is becoming clear; however, our understanding of the underlying structural and biochemical properties that govern HLA-F function is limited. Molecular modeling and sequence alignment has predicted that HLA-F shares the highly conserved MHC fold but with a partially open-ended groove (Goodridge et al., 2010). In the MHC-I family there are ten conserved residues that are critical for establishing the architecture of the groove and for specific interactions with peptide residues. Five of these ten residues are altered within the HLA-F groove, which has led to the prediction that HLA-F either does not present peptide or it does so in a fundamentally divergent manner from other HLAs (Geraghty et al., 1990). Meticulous studies have failed to elute canonical MHC-I-like peptides from natively expressed HLA-F in human cell lines. Thus, it is generally thought that HLA-F does not present antigen (Goodridge et al., 2010;

Wainwright et al., 2000) and instead may function as an empty, open conformer (OC) that heterodimerizes with other MHC-I molecules and lacks association with beta-2 microglobulin (β_2m) (Goodridge et al., 2013). However, there is evidence for dimerized HLA-F complexed with β_2m on the cell surface of placental tissues during pregnancy (Hackmon et al., 2017) and small amounts of β_2m-HLA-F have been extracted from cells (Goodridge et al., 2010). Furthermore, HLA-F interacts with components of the transporter associated with antigen processing (TAP) peptide-loading complex (Lepin et al., 2000; Wainwright et al., 2000). This suggests that HLA-F may exist in multiple isoforms with varying potential for peptide binding and recognition by antigen receptors.

Previous studies indicate that HLA-F can regulate immunity through direct interactions with NKRs. Like other MHC-I molecules, HLA-F binds NKRs from the LIR and KIR families: LIR1, LIR2 (Lepin et al., 2000), KIR2DS4, KIR3DL2 (Goodridge et al., 2013), KIR3DL1 and KIR3DS1 (Garcia-Beltran et al., 2016). However, since these studies were conducted with denatured and refolded HLA-F, the possible contribution of bound peptide in these interactions has not been explored. The molecular mechanism for HLA-F recognition by NKRs is also entirely unclear as there have been no published studies on HLA-F structure.

Here, we present a molecular description of HLA-F and its recognition by an inhibitory NKR and elucidate the importance of peptide binding for differential NKR reactivity. Our structural, biochemical and evolutionary analyses establish that HLA-F can exist as both an OC and as a bona fide peptide-presenting MHC molecule. Our cellular assays and binding studies confirm the functional significance of HLA-F and provide a model for how peptide binding modulates HLA-F recognition by activating and inhibitory NKRs. Altogether, these data have major implications for our understanding of how HLA-F functions as an immunoregulatory molecule.

Results

The crystal structure of HLA-F reveals strong evidence for a unique mode of peptide presentation

The β_2m-HLA-F fusion construct was produced in High Five (Hi5) cells via the baculovirus insect cell expression system and yielded crystals that diffracted to 2.62 Å. The structure of HLA-F was solved in two different space groups by molecular replacement with HLA-B27 (Madden et al., 1992). Consistent with the high degree of structural homology in the MHC-I family, HLA-F adopts a conserved overall architecture and associates with β_2m via a conventional interface (Figure 1A). At first glance, the antigen-binding groove of HLA-F is quite canonical; alignment with HLA-A2 and HLA-G yields root mean square deviations (RMSD) of only 0.53 Å and 0.763 Å (Cα of residue 1-180) with ~77% sequence identity (Figure 1B). The molecular landscape of the HLA-F groove, with a volume of ~1250 $Å^3$, is more consistent with the peptide-presenting MHC-I molecules than the non-peptide-presenting MHC-like molecules, MICA and FcRN, which have collapsed grooves (Figure 1C).

Consistent with peptide presentation, $2F_o$-F_c electron density and composite omit maps reveal a large continuous tube of electron density in the groove that is not attributed to any of

the residues of HLA-F (Figure 2). A peptide of approximately 8 residues can be modeled into this extra density but due to the heterogeneous nature of bound peptides, the exact identities of the peptide side-chains are unclear. Indeed, when interrogated via liquid chromatography-mass spectrometry (LC-MS), HLA-F produced in this system was found to contain 48 distinct peptides that did not originate from the HLA-F construct or a common contaminant, keratin (Table S2). However, only one peptide hit the Hi5 source organism (*Trichoplusia ni*), likely because the protein database for *Trichoplusia* is small, consisting of only 216 protein sequences. Thermal denaturation revealed that peptide-loaded Hi5-derived HLA-F has a melting temperature (Tm) in line with the most stable MHC-I-peptide complexes observed (Figure S1) (Morgan et al., 1997).

Due to the unique molecular landscape of the HLA-F groove, the placement of the bound peptide is distinct compared to how other MHC-I molecules present peptide. The canonical MHC-I binding pockets (A–F) described for HLA-A2 (Saper et al., 1991) (Figure 2A) that dictate specificity for interactions with peptide side-chains are substantially altered in the HLA-F groove due to the substitution of five of the ten aforementioned highly conserved residues in MHC-I molecules (Figure S2). These substitutions modify the electrostatic environment and hydrogen-bonding network in the groove. Nonconservative amino acid alterations at two additional positions, G62W and G26E, result in an entirely blocked off A pocket which forces the unanchored N-terminus of the peptide to snake up and out of the groove. In the absence of an N-terminal anchor, the central (P5) and C-terminal (P7 and P8) portions of the peptide are firmly anchored within the C, E and F pockets via hydrogen bonds to the peptide backbone and side-chains (Figure 2C). The central pocket (C) is formed by a pronounced substitution to a glycine at position 97, which is occupied by a tryptophan or bulky, charged residue in all other MHC-I molecules. The electron density of the peptide residue that is anchored deep within this pocket is evocative of a bulky residue such as a tryptophan but is also consistent with a post-translationally modified (PTM) side-chain (Figure 2C). This residue is coordinated by a His114-His116 motif that is reminiscent of the His-His motif seen in the groove of HLA-E (O'Callaghan and Bell, 1998) as well as those seen in the active sites of histidine phosphatases where they are essential for coordinating the substrate phosphate for catalysis.

HLA-F presents endogenous peptides of a length distribution reminiscent of MHC class II (MHC-II) molecules

The crystal structure of HLA-F led us to question whether its divergent topography and peculiar peptide orientation would have ramifications on the size and types of peptides that HLA-F can present. To investigate HLA-F peptide presentation in human cells, we recombinantly expressed and purified soluble HLA-F from HEK293T (293T) cells for peptide elution analysis via mass spectrometry. Secreted 293T HLA-F has a melting curve that is consistent with those reported for other MHC-I molecules bound with endogenous peptides and expressed in a similar manner (Figure S1) (Fahnestock et al., 1992).

MHC-Ia molecules bind an impressive variety of peptides (elution samples from a similar quantity of MHC-I contain >5,000 peptides (Trolle et al., 2016)) while peptide elution experiments from the more specialized MHC-Ib proteins typically identify much fewer

peptides (Kraemer et al., 2015). 2,679 peptide sequences were eluted from WT HLA-F produced in 293T cells and identified with high confidence by liquid chromatography-mass spectroscopy (LC-MS) (Table S3). In agreement with the structural evidence that HLA-F peptides are not constrained by the length of the groove, peptides eluted from HLA-F are much longer than the typical length of MHC-I peptides (8-10 residues). HLA-F peptides range from 7 residues to >30, peaking at 12 residues. This length distribution is more consistent with that of MHC-II molecules (Figure 3A) (Bergseng et al., 2014), which escape the length constraints imposed on peptides by having a groove that is open at both ends (Brown et al., 1993). Consistent with the structural data showing that HLA-F peptides lack N-terminal anchors, the peptide motif analysis suggests that HLA-F is relatively unselective aside from a preference for a charged residue (such as an aspartate) at the most C-terminal position (Figure 3B). This C-terminal residue is firmly anchored via a hydrogen bond from T143 to the peptide backbone as well as two salt bridges from R84 to the peptide side-chain and backbone (Figure 2C). This C-terminal anchoring strategy is unique to HLA-F, as all other MHC-I molecules have a tyrosine at position 84 that makes a single hydrogen bond with the C-terminus of the peptide backbone.

While HLA-F largely conforms to the principles of MHC-I peptide presentation in terms of the source proteins sampled (Figure S3), the 2D LC-MS data indicates that peptides bound by HLA-F have a high prevalence of PTMs, particularly phosphorylation (Figure 3C). This data, accompanied by the observation of the His-His motif in the C pocket suggests that HLA-F may be able to accommodate a phosphorylated side-chain deep in the center of the groove.

The R62W substitution converts HLA-F into a peptide-presenting molecule

The peptide elution data prompted us to consider the evolutionary processes that led to such a divergent molecular landscape and mode of peptide presentation. Our analysis suggested that HLA-F peptide presentation evolved independently in the human and orangutan lineages with the convergent substitution of arginine62 to tryptophan (R62W) (Figure 4A). This substitution, which is absent in chimpanzee, gorilla and other primate versions of HLA-F, is the only nonconservative amino acid change between the groove of human and chimpanzee HLA-F. Modeling the selective pressure acting on the *HLA-F* gene in primates with a PRoperty Informed Model of Evolution (PRIME) using the Conant-Stadler amino acid categories (Conant et al., 2007) suggested the strong change in polarity of the R62W substitution was positively selected whereas other positions in the groove have remained constant over time via purifying selection (Table S4). Mutation of W62 to the ancestral R (W62R) almost completely abolished peptide binding. Only 53 peptides were eluted and identified by LC-MS from W62R HLA-F, which was expressed and purified from 293T cells in the same manner as WT (Figure 4C). This reduction was seen in both the diversity of peptides (~98% reduction) and the total quantity of peptide bound (~90% reduction) as represented by the summed ligand intensity for all eluted peptides. Considering that the R62W substitution only exists in human and orangutan HLA-F, it is likely that other primate versions of HLA-F lack peptide presentation. Other substitutions among primate versions of HLA-F may also be functionally important, such as those on the right side of the groove that may alter the KIR footprint (Figure 4B).

High affinity recognition of β_2m-HLA-F by LIR1 is mediated via a docking strategy shared with the viral UL18 MHC mimic

We used Blitz biolayer interferometry (BLI) to measure interactions between HLA-F and the inhibitory NKR, LIR1. Previous studies characterizing this interaction utilized empty β_2m-HLA-F produced through refolding of *E.coli*-generated inclusion bodies and did not report affinity measurements (Lepin et al., 2000). For our binding experiments, we produced HLA-F OC through refolding and peptide-loaded β_2m-HLA-F in 293T or Hi5 cells and LIR1 D1–D2 was also made in Hi5 cells. While LIR1 does not bind HLA-F OC with a measureable affinity (Figure S4A), it recognizes peptide-bound β_2m-HLA-F with an equilibrium KD of 2 μM (Figure 5B), which makes β_2m-HLA-F the highest affinity ligand for LIR1 among the human MHC-I molecules (affinities range from 15–100 μM (Chapman et al., 1999)).

To investigate the molecular details of this interaction we crystallized and solved the complex structure of LIR1 bound to HLA-F (Figure 5A). The structure revealed that LIR1 adopts a highly conserved docking orientation on the side of the β_2m-HLA-F complex that was also seen in the existing HLA-A2–LIR1 (Willcox et al., 2003), UL18–LIR1 (Yang and Bjorkman, 2008) and HLA-G–LIR2 (Shiroishi et al., 2006) complex structures (Figure 5C). The HLA-F–LIR1 interface has ≈1,700 Å^2 total solvent-accessible surface area buried, which is nearly identical to that of the HLA-A2–LIR1 interface and less than the ≈2,200 Å^2 UL18–LIR1 interface. Owing to the docking orientation of LIR1 on the side of HLA-F away from the peptide-presenting groove, the affinity of LIR1 for the ancestralized W62R β_2m-HLA-F is only slightly reduced (Figure S4B). This result is in agreement with previous reports that MHC–LIR ligation is not directly dependent on interactions with peptide (Willcox et al., 2003), although peptide is required for stable surface expression of the mature β_2m-MHC-I-peptide complex (Blum et al., 2013).

The interactions between MHC-I and LIR1 can be separated into two separate interfaces; the interface where the D1–D2 hinge region contacts β_2m (site 1) and the interface where residues of the MHC-I α3 domain are recognized by the LIR1 D1 domain (site 2) (Figure 5A). The site 1 interface is entirely conserved in LIR1 recognition of MHC-I family members, which may explain why LIR1 binding to HLA-F OC is greatly reduced. While there are some amino acid differences between the α3 domain of HLA-F and HLA-A2 at the site 2 interface, these changes don't greatly alter the chemical properties of the residues (i.e. I200 vs V200). A conformational change in the UL18 binding loop of LIR1 (which is mostly unstructured in the HLA-A2–LIR1 complex) allows it to engage the tip of the α3 domain of HLA-F via two salt bridges (HLA-F D196–LIR1 R84 and HLA-F E229–LIR1 K41), two hydrogen bonds (HLA-F D196–LIR1 D80 and HLA-F P193–LIR1 T43) and numerous van der Waals contacts (Figure 5A) (Figure S5) (Table S5). These additional contacts are reminiscent of high affinity LIR1 recognition of the viral MHC mimic, UL18 (Figure 5C, **right inset)**. Adoption of this modified recognition strategy might explain why LIR1 has a greater affinity for β_2m-HLA-F than any other MHC-I molecule measured.

Peptide binding prevents HLA-F recognition and triggering of KIR3D

In order to assess whether peptide-bound HLA-F can bind to and trigger signaling of KIRs previously shown to recognize HLA-F OC, we employed a Jurkat reporter cell (JRC)

system. To this end, we used β_2m-deficient Jurkat cells stably transduced with KIR chimeric constructs (KIRζ) containing the extracellular and transmembrane domain of the KIR of interest and the cytoplasmic domain of CD3ζ. This allows for measurement of CD69 expression as an activation marker following functional ligation of the transduced KIR (Figure 6C). For KIR3DS1 and KIR2DS4, we used the transmembrane domain of KIR3DL1 to ensure stable cell-surface expression independent of the DAP12 adaptor protein. We confirmed surface expression of KIRζ on Jurkat cells via antibody staining (Figure 6D). Reporter cells were then incubated with cell-sized beads coated with biotinylated monomers of HLA-F. Antibody-mediated crosslinking of KIRζ-JRC served as a positive control whereas streptavidin beads coated with free biotin and JRCs expressing an irrelevant KIRζ (KIR2DL3) were used as negative controls.

Upon bead binding, granularity of the cells increased substantially, which allowed for discrimination of bead-bound from unbound cells. HLA-F OC beads bound to KIR3DS1ζ-JRC and KIR3DL2ζ-JRC to a similar extent as beads coated with their respective anti-KIR antibodies (Figure 6A) and triggered activation in line with previous findings (Figure 6B) (Garcia-Beltran et al., 2016). Beads coated with peptide-bound HLA-F produced in 293T or Hi5 cells did not bind or activate KIR3DS1ζ-JRC or KIR3DL2ζ-JRC. In addition, our findings assert that HLA-F is not a ligand for the activating KIR2DS4 as no binding or HLA-F-mediated triggering was detected with KIR2DS4-JRC. This was irrespective of HLA-F peptide status and contrary to what was previously reported (Goodridge et al., 2013). Overall, these results suggest that unlike HLA-F OC, peptide-bound HLA-F is not a ligand for KIR3DS1 and KIR3DL2 and perhaps, peptides directly hinder HLA-F–KIR ligation.

Tetramers composed of HLA-F loaded with endogenous peptides or HLA-F OC differentially stain leukocytes

To explore potential receptors that might be responsive to peptide-loaded HLA-F ex vivo, we made tetramers from HLA-F protein produced in 293T cells. We compared peripheral blood mononuclear cell (PBMC) staining of these tetramers with those made from HLA-F expressed in Hi5 cells (which is bound with insect peptides) or HLA-F OC (which is empty and lacking β_2m) and drew tetramer$^+$ gates using our negative control T22 tetramers.

Fresh PBMCs obtained from 4 healthy volunteers were stained with a panel of lymphocyte and monocyte markers as well as antibodies detecting LIR1, KIR3DS1-L1 and KIR3DL2 before tetramer staining. LIR1 expression on a wide range of leukocytes was consistent with previous reports (Colonna et al., 1997); 8–53% of CD56$^+$-CD16$^+$ NK cells, 4–8% of CD3$^+$ T cells, 75–95% of B cells and nearly all monocytes express LIR1 (Figure S6). KIR3DS1-L1 expression on NK cells (10–35%) and T cells (.7–2%) was also consistent with previous studies (O'Connor and McVicar, 2013), but surprisingly, KIR3DL2 expression could not be detected in our donor pool.

Tetramer staining of PBMCs revealed that HLA-F tetramers consistently stained a broad array of cell types and that peptide presentation has a dramatic effect on the staining profile. Peptide-bound 293T tetramers stained a statistically significant greater proportion of T cells (~2.5-fold), NK cells (~4-fold), and monocytes (~4-fold) than HLA-F Hi5 tetramers (Figure 7). The HLA-F OC tetramers do not markedly stain T cells. However, consistent with

interactions with NKRs, HLA-F OC tetramers stained a greater proportion of B cells (~3-fold) and NK cells (~2-fold) compared to Hi5 tetramers. Although not statistically significant, the data also show a clear trend for greater 293T tetramer staining of T cells and NK cells compared to OC tetramers, suggesting that recognition is enhanced when HLA-F is loaded with peptides of human origin. It seems that a substantial portion of the tetramer staining with 293T and OC HLA-F cannot be attributed to interactions with known HLA-F binding partners, as $LIR1^+$ T cells and $KIR3DS1\text{-}L1^+$ NK cells show only slightly greater tetramer staining (Figure S6C). Therefore, this increase in tetramer staining may be due to interactions with unexplored HLA-F receptors, such as TCRs and KIRs, that sense peptide-dependent changes in HLA-F surface epitopes.

Discussion

Prior to this study, it was unclear if HLA-F presented antigen, despite its strong resemblance to other members of the MHC-I family and painstaking efforts to address this question. Structural biology has allowed us to peer into the groove of HLA-F and visualize the molecular landscape that has been remodeled through evolution for a specialized mode of peptide presentation. The extra electron density we see in the antigen-binding groove of HLA-F is reminiscent of what Bjorkman and Wiley reported when they solved the first structure of an MHC molecule (Bjorkman et al., 1987). However, HLA-F evolved substitutions in the groove that have molded it into an open-ended cleft capable of presenting long peptides that extend up and out of the groove. One substitution, R62W, which arose separately in the human and orangutan lineages, imparts HLA-F with the ability to present these noncanonical peptides, allowing for a dramatic change in function over a relatively short period of time.

This study motivates further examination of the biochemical and functional transformation of the HLA-F groove in primate evolution. What is the most ancient, functionally significant HLA-F orthologue and in what context did it regulate immunity, via antigen presentation or another means? Throughout primate evolution, pregnancy has progressively become more invasive and immunologically complex (Coe and Lubach, 2014; Carter et al., 2015). The distinct expression pattern of HLA-F (Shobu et al., 2006; Hackmon et al., 2017) and its ability to regulate NK cells which govern the remodeling of the fetal-maternal interface during pregnancy, indicate a role for HLA-F during gestation. Future studies will supplement the abundant observational evidence that HLA-F plays a critical role in pregnancy by providing mechanistic insight into how and through which NKRs HLA-F regulates gestational immunity.

Previous studies attempting to elute canonical peptides from HLA-F have relied upon purified, native HLA-F from unstimulated, uninfected cell lines where surface expression is tightly regulated and HLA-F is predominately intracellular and empty (Wainwright et al., 2000). Protein engineering and recombinant expression strategies allowed us to capture HLA-F in a peptide-receptive state that may be, to a greater extent, free from regulatory checkpoints for antigen-loading and trafficking. This enabled us to examine large quantities of HLA-F for evidence of peptide presentation and allowed for the confident identification

of unconventional peptides that may have been previously overlooked due to their large size (Goodridge et al., 2010).

Though we have clearly shown that HLA-F can present peptide, the mechanism of peptide-loading and functional consequences of peptide presentation require further study. The role of the open-ended groove of HLA-F that causes extension of the N-terminal portion of HLA-F peptides is also unclear and future studies will determine if these extended peptides are engaged by antigen receptors. Another unexplained facet of HLA-F peptide presentation is the prevalence of PTMs on peptides eluted from HLA-F. Could these chemically altered residues substantially influence the epitopes seen by antigen receptors and has HLA-F evolved a groove that is particularly well-suited for presenting phosphorylated peptides? This notion is evocative of peptide presentation by the rodent MHC molecule, H2-M3, which has a groove that is specialized for presenting bacterial N-formyl peptides (Wang et al., 1995).

Our Jurkat reporter assay validated previous reports that HLA-F OC are a ligand for KIR3D and demonstrate that HLA-F OC and peptide-bound HLA-F have distinct NKR binding partners. This indicates that peptide binding directly obstructs HLA-F recognition by KIR3D or it alters the anatomy of the HLA-F groove and the molecular epitopes seen by NKRs. Like TCRs, NKRs can be highly sensitive to presented peptides; KIR3D are generally thought to rely directly on interactions with the P7 and P8 residues of bound peptides for MHC-Ia recognition (O'Connor et al., 2015) yet they recognize HLA-F OC devoid of peptide and do not bind HLA-F presenting endogenous peptides. However, the relatively low Tm for 293T-expressed HLA-F suggests that HLA-F secreted from 293T cells may not be bound with ideal peptide ligands. Future studies will explore conditions, such as in pregnancy, cancer or infection, where HLA-F will have access to different peptide sources that could influence its reactivity with antigen receptors.

Our tetramer staining studies expand our view of how peptide binding influences how antigen receptors see HLA-F. These data justify further exploration of antigen-specific recognition of HLA-F by TCRs and NKRs. However, the broad staining of leukocytes by peptide-loaded and OC tetramers suggests that the bulk of receptors that engage HLA-F are not particularly reliant on peptides and are highly conserved across cell types and donors, such as the LIRs. Consistent with an extensive immunoregulatory role, LIR1 recognition of MHC-Ia and HLA-G inhibits the cytotoxicity and activation of NK cells and other leukocytes in a variety of settings (Colonna et al., 1997; Favier et al., 2010). In HLA-F recognition, the highly-conserved MHC-I–LIR footprint is supplemented with an additional interaction interface that is also seen in the UL18–LIR1 complex structure. We propose that the enhanced affinity of LIR1 for HLA-F can be attributed to this additional contact site that is absent in other examples of LIR1–MHC-I recognition.

Our thermal denaturation assays show that HLA-F OC, with a Tm of 52°C, are thermo-stable compared to other empty MHC-I molecules tested previously (Tm range 40–45°C) (Strong et al., 2003). The ability to exist in an OC and peptide-bound state, equips HLA-F with an additional layer of regulatory potential that is unique in the MHC-I family. However, it is unclear what regulates the switching of HLA-F from an OC to a peptide-bound state. Is

it the availability of ligand, as is the case for other members of the MHC-I family (Lee et al., 1998) or could environmental conditions, such as changes in pH that occur during infection or inflammation, modulate the conformation of HLA-F on the cell surface? Further study is needed to describe the molecular architecture of MHC-I OC and how they are recognized by NKRs. Elucidation of this mechanism will be a critical step toward understanding how KIRs can engage peptide-bound MHC-Ia molecules as well as HLA-F OC. Perhaps cell-surface association with MHC-Ia molecules, with or without peptide, plays an important role in HLA-F OC recognition (Goodridge et al., 2010).

Evidence is mounting that HLA-F signaling through NKRs regulates the immune system in pregnancy, infection and autoimmunity. Until recently, our understanding was limited of the underlying structural and biochemical properties that govern HLA-F function. The data presented in this study has changed our general understanding of the evolution of antigen presentation within the context of the MHC. Our results provide a blueprint of the molecular details of HLA-F, which will inform future exploration of its roles in human health and allow for the development of additional, targeted therapeutics.

STAR Methods

Contact for Reagent and Resource Sharing

Further information and requests for reagents should be directed to and will be fulfilled by the Lead Contact, Erin J. Adams (ejadams@uchicago.edu).

Experimental Model and Subject Details

Human subjects—Samples of peripheral blood were obtained from healthy volunteers under protocols approved by the ethical committees of the University of Chicago (IRB13-0666). The cohort was composed of two male and two female donors aged 24–30 years.

Cell lines—Sf9 insect suspension cells (*Spodoptera frugiperda*, female, ovarian) grown in Sf-900 II SFM supplemented with heat-inactivated FBS (to 10%), L-glutamine (to 1%) and Gentamicin Sulfate (.01 mg/mL) were used for production of baculovirus. High Five insect suspension cells (*Trichoplusia ni*, female, ovarian) grown in Insect-XPRESS Protein-free Insect Cell Medium supplemented with L-glutamine (to 1%) and Gentamicin Sulfate (.01 mg/mL) were used for protein production. All insect cell cultures were grown at 27°C with 120 rpm shaking. Human embryonic kidney HEK293T adherent cells were grown at 37°C in 5% CO_2 in culture medium composed of Advanced DMEM, 2% heat-inactivated ultra-low Ig FBS, antibiotic/antimycotic and 2mM L-glutamine. The Jurkat cell line (clone E6.1) was cultured at 37°C in 5% CO_2 in RPMI-1640 containing L-glutamine supplemented with 20% FBS Superior and 1 μg/ml Puromycin.

Bacteria—*E. coli* BL21(DE3), DH5α and Rosetta(DE3) pLysS were cultured at 37°C, shak ing at 250 rpm.

Method Details

Cloning, protein expression and purification—For Hi5 insect cell and 293T expression, the extracellular portion of the mature HLA-F (Gly1-Ile284) was fused to β_2m (Ile1-Met99), as described previously (Godeau et al., 1992), with a 15 residue Gly-Ser linker (GGGGSGGSGSGGGS) via overlapping PCR.

HLA-F (GenBank: BC062991.1):
MAPRSLLLLLSGALALTDTWAGSHSLRYFSTAVSRPGRGEPRYIAVEYVDDTQFLRFD
SDAAIPRMEPREPWVEQEGPQYWEWTTGYAKANAQTDRVALRNLLRRYNQSEAGS
HTLQGMNGCDMGPDGRLLRGYHQHAYDGKDYISLNEDLRSWTAADTVAQITQRFY
EAEEYAEEFRTYLEGECLELLRRYLENGKETLQRADPPKAHVAHHPISDHEATLRCW
ALGFYPAEITLTWQRDGEEQTQDTELVETRPAGDGTFQKWAAVVVPSGEEQRYTCH
VQHEGLPQPLILRWEQSPQPTIPIVGIVAGLVVLGAVVTGAVVAAVMWRKKSSDRNR
GSYSQAAV

β_2m (NG_012920.1):
MSRSVALAVLALLSLSGLEAIQRTPKIQVYSRHPAENGKSNFLNCYVSGFHPSDIEVD
LLKNGERIEKVEHSDLSFSKDWSFYLLYYTEFTPTEKDEYACRVNHVTLSQPKIVKW
DR DM

For crystallography, β_2m-HLA-F and the D1–D2 domains of LIR1 (Gly24-Gly198) were cloned into the baculovirus insect cell expression vector, pACgp67A, modified to contain an N-terminal 8x his-tag and a 3C protease site (HHHHHHHH-GSGGLEVLFQGP) downstream of the gp67A secretion signal sequence (MLLVNQSHQGFNKEHTSKMVSAIVLYVLLAAAAHSAFA).

LIR1 (GenBank: ADJ55948.1):
MTPILTVLICLGLSLGPRTHVQAGHLPKPTLWAEPGSVITQGSPVTLRCQGGQETQEY
RLYREKKTALWITRIPQELVKKGQFPIPSITWEHAGRYRCYYGSDTAGRSESSDPLELV
VTGAYIKPTLSAQPSPVVNSGGNVILQCDSQVAFDGFSLCKEGEDEHPQCLNSQPHA
RGSSRAIFSVGPVSPSRRWWYRCYAYDSNSPYEWSLPSDLLELLVLGVSKKPSLSVQ
PGPIVAPEETLTLQCGSDAGYNRFVLYKDGERDFLQLAGAQPQAGLSQANFTLGPVS
RSYGGQYRCYGAHNLSSEWSAPSDPLDILIAGQFYDRVSLSVQPGPTVASGENVTLL
CQSQGWMQTFLLTKEGAADDPWRLRSTYQSQKYQAEFPMGPVTSAHAGTYRCYG
SQSSKPYLLTHPSDPLELVVSGPSGGPSSPTTGPTSTSGPEDQPLTPTRSDPQSGLGRH
VGVVIGILVAVVLLLLLLLLLFLILRHRRQGKHWTSTQRKADFQHPAGAVGPEPTDR
GLQWRSSPAADAQEENLYAAVKHTQPEDGVEMDTRQSPHDEDPQAVTYAEVKHSRP
RREMASPPSPLSEEFLDTKDRQAEEDRQMDTEAAASEAPQDVTYAQLHSLTLRREAT
EP PPSQEGPSPAVPSIYATLAIH

For BLI measurements and tetramer production, HLA-F constructs and LIR1 D1–D2 were cloned into vectors containing a BirA biotinylation sequence (Avitag) upstream of a 3C protease site and 8x his-tag (GLNDIFEAQKIEWHE-GGSG-LEVLFQGP-HHHHHHHH). For production of refolded HLA-F OC and β_2m-HLA-F, the extracellular portion of HLA-F (Gly1-Ile284) and β_2m (Ile1-Met99) were separately cloned in frame with methionine start codons in the pET28a vector. Bacterial inclusion bodies were generated in *E. coli*

BL21(DE3) and Rosetta(DE3) pLysS and refolded essentially as described previously (Garboczi et al., 1992; O'Callaghan et al., 1998) with omission of peptide.

Hi5 cells were grown in 1 L volumes in 2.4 L flasks and transduced with high titer recombinant baculovirus (P2) stock generated in Sf9 cells at a 1:1000 dilution. 72 hours after infection, the culture media was collected and his-tagged protein secreted into the media was extracted via overnight (O/N) batch binding at 4°C with Nickel agarose (nickel-nitrilotriacetic acid (NTA)) in the presence of 20 mM imidazole, pH 7 to reduce non-specific binding. Proteins were eluted with 200 mM imidazole, pH 8 in HBS, buffer exchanged to HBS buffer via disposable desalting columns and incubated with 3C protease (1:100) for cleavage of his-tags O/N at 4°C. HBS buffer is composed of 10 mM HEPES, pH 7.2, 150 mM NaCl and 0.02% NaN3. Proteins were further purified by Superdex S200 size-exclusion chromatography FPLC in HBS buffer. Refolded protein was purified similarly via Ni-NTA and size exclusion chromatography in HBS buffer. Protein concentration was initially determined by BCA and matched A_{280} measurements using theoretical extinction coefficients (calculated by the ExPASy Protparam tool). For immobilization on streptavidin biosensors, the Avitag constructs were biotinylated with BirA biotin protein ligase in the presence of biotin, and subsequently purified via size exclusion chromatography. The HLA-F W62R mutant was cloned by overlapping PCR using the WT construct as a template and was purified similarly. For crystallization, peak fractions of β_2m-HLA-F were concentrated to 6 mg/mL and peak fractions of LIR1 were concentrated to 3 mg/mL. For HLA-F–LIR1 complex formation, HLA-F and LIR1 were mixed at a 1:1 molar ratio and incubated at room temperature for 1 hour before being concentrated to 7.5 mg/mL.

Crystallization and structure determination—β_2m-HLA-F at 6 mg/mL was crystallized using hanging drops at 20°C by mixing 1:1 or 1.4:1 with mother liquor (ML) containing 27% PEG 10000 and 0.1 M Tris, pH 8.5. HLA-F–LIR1 at 7.5 mg/mL was crystallized via hanging drops by mixing 1:1 or 1.4:1 with ML containing 27% PEG 550 MME, 0.1 M Tris, pH 7 and 300 mM NaCl. Crystals were cryo-cooled in ML supplemented with 10–20% (v/v) glycerol, 10–20% (v/v) ethylene glycol or 35% PEG 550 MME before data collection. The β_2m-HLA-F datasets were collected on a MAR300 CCD detector at beamline 23 ID-B and the β_2m-HLA-F–LIR1 datasets were collected on a Dectris Pilatus3 6M detector at beamline 23 ID-D at the Argonne National Laboratory Advanced Photon Source. Datasets were processed with Xia2 (Winter, 2010) and solved by molecular replacement with the program Phaser (McCoy et al., 2007) using the following search models for each structure: HLA-F - PDB ID: 1HSA (Madden et al., 1992) and HLA-F–LIR1 - PDB ID: 1P7Q (Willcox et al., 2003). For both structures, Phenix (Adams et al., 2010) was used for initial rigid body refinement and then for subsequently restrained refinement of individual sites and B-factors. Non-crystallographic restraints were applied for the HLA-F structure as there are four copies of β_2m-HLA-F in the asymmetric unit. Between refinement cycles, manual model building was performed with COOT (Crystallographic Object-Oriented Toolkit). Ligand-placing was guided by $2F_o$-F_c, F_o-F_c and composite omit maps generated with Phenix. Analysis of buried surface area was conducted with the program PDBePISA (http://www.ebi.ac.uk/msd-srv/prot_int/cgi-bin/piserver) and areaimol (CCP4). Data collection and refinement statistics can be found in Table S1. For the HLA-F structure,

chains I (HLA-F), J (β_2m) and N (peptide) were used to make figures and the side-chains of HLA-F residues 42 and 177 were modeled as alanines due to poor resolution of side-chains. For the HLA-F–LIR1 structure, the side-chains of HLA-F residues 44, 85, 121, 123, 133, 137 and 169; β_2m residue 2; LIR1 residues 2, 27, 32, 42, 49, 57, 59, 74, 135, 136, 141, 170, 172, and 193; and peptide residues 2 and 3 were modeled as alanines. Contacts between HLA-F and LIR1 were calculated with the program Contacts (CCP4 (Winn et al., 2011)) using cut-offs for hydrogen bonds, Van der Waals, and salt-bridges of 3.5, 4.0, and 4.5 Å, respectively. RMSD calculations and structure representations were conducted with PyMol (The PyMOL Molecular Graphics System, Schrödinger, LLC.).

Production of HLA-F in 293T cells—After failed attempts to express large quantities of untagged HLA-F in human cells we began multiple iterations of protein engineering that produced the N-terminal monomeric superfolder green fluorescent protein (msGFP) β_2m-HLA-F 293T fusion construct. The N-terminal msGFP greatly enhanced the yield of HLA-F from 293T cells, consistent with previous reports of N-terminal fusion partners, such as maltose binding protein (MBP), increasing the solubility and yield of aggregation-prone proteins (Raran-Kurussi et al., 2015). To our knowledge, this is the first report utilizing N-terminal GFP fusion as a protein yield amplification strategy in large-scale protein production.

To create the HLA-F 293T construct, β_2m-HLA-F was modified via the addition of the native HLA-F signal peptide (MAPRSLLLLLSGALALTDTWA) followed by a Gly-Ser linker (GSGSSGSSGSSGSS), msGFP (MDSTESLFTGVVPILVELDGDVNGHKFSVRGEGEGDATNGKLTLKFICTTGKLPVP WPTLVTTLTYGVQCFSRYPDHMKQHDFFKSAMPEGYVQERTITFKDDGTYKTRAEV KFEGDTLVNRIELKGIDFKEDGNILGHKLEYNFNSHNVYITADKQKNGIKANFKIRH NVEDGSVQLADHYQQNTPIGDGPVLLPDNHYLSTQSKLSKDPNEKRDHMVLLEFV TAAGITH) (Fitzgerald and Glick, 2014) and a C-terminal 8x his-tag. A similar construct containing a 3C protease site downstream of the msGFP and a C-terminal Avitag upstream of a 3C protease site and 8x his-tag was created for production of HLA-F 293T tetramers.

293T cells were grown in 150 cm^2 tissue culture plates with grid in a humidified tissue culture incubator (37°C, 5% CO_2) and transient transfection via polyethylenimine (PEI) and protein production was performed essentially as described previously (Smith et al., 2009). 12 hours after transfection, media was changed to basal media containing 250 mL each of sterile RPMI and DMEM; 3.75 mL of Antibiotic/Antimycotic (100x) and 5 mL each of L-glutamine (200 mM), Nutridoma SP (100x) and sodium pyruvate (100 mM).

Purification of protein secreted into the culture media was performed 4–5 days after transfection as described previously (Aricescu et al., 2006). W62R HLA-F was expressed and purified from 293T cells similarly. Protein yields of 1–3 mg protein per 500 mL culture media were typical. Biotinylated monomer was purified via Ni-NTA and size exclusion chromatography. Peak fractions were pooled and concentrated to 1–2 mg/mL and tetramer preparation was performed as described by the NIH tetramer core facility via incubation of biotinylated monomer stocks with a 1.1 molar excess of streptavidin-APC.

Thermal denaturation of HLA-F constructs—HLA-F protein was produced via Hi5 insect cell expression, 293T cell expression, or through refolding of bacterial inclusion bodies and subjected to thermal melting within 24 hours of purification. The CD signal at 222 nm was monitored on a JASCO J-1500 CD spectrometer equipped with a Peltier-thermo cell holder. Data were obtained from samples containing 10–20 μM HLA-F in HBS buffer as the temperature was raised from 26°C to 86°C in 2 degree intervals at a rate of 2°C/minute with a 2 minute equilibration time, and 1 nm bandwidth. CD data was fit with a 4-parameter sigmoidal curve with Prism and Tms were calculated as the half-point of the ellipticity change between the native and denatured states. CD data were normalized to the IC β_2m-HLA-F curve. For all Tms, the std. error is less than ±1.8°C.

Peptide identification using nano-scale LC-MS—For the *de novo* identification of peptide ligands; 0.8 mg of HLA-F produced in Hi5 cells was used; 2.5 mg of WT HLA-F or 1.2 mg of W62R HLA-F produced in 293T cells was used. Ligands were isolated from HLA-F as previously described (McMurtrey et al., 2016, Trolle et al., 2016 and Yaciuk et al., 2014). Briefly, the isolated ligand pool was fractionated using pH 10 reverse-phase HPLC, described in detail previously (Yaciuk et al., 2014). Each fraction was dried and resuspended in 10% acetic acid for LC-MS.

Approximately 50% of each HPLC fraction was injected into a nano-scale reverse phase liquid chromatography Eksigent nano-LC-4000 (Sciex) system. Column specifications, mobile phase solvents, and elution gradient are previously described in detail (Trolle et al., 2016). Spectra were acquired in data-dependent acquisition (DDA) mode. DDA spectra from all of the fractions were interpreted using PEAKS v7.0 or v8.0 (Bioinformatic Solutions) and were searched against the Uniprot *Homo sapiens* or *Trichoplusia ni* database at <=1% FDR. A maximum of 2 variable modifications per peptide were allowed and included: N-terminal acetylation, deamidation (N, Q), Oxidation (M, W, H), Pyro-glu from Q, Cysteinylation (C), Sodium adduct (c-term, D, E), Phosphorylation (T, S, Y). Peptides originating from the HLA-F construct were removed from the ligand list as these are known acid hydrolysis products. Peptide intensity was determined from the MS1 precursor ion area underneath the curve using Skyline v3.1 and was normalized to the input quantity of HLA-F. Ligands were sorted by amino acid length and a motif was generated using the online tool Seq2Logo (http://www.cbs.dtu.dk/biotools/Seq2Logo/) with the default settings. Letters represent the standard single letter abbreviation for an amino acid. The size of the letter represents the overrepresentation (positive bits) or underrepresentation (negative bits) of that amino acid compared to the naturally occurring frequency of the respective amino acid.

Evolutionary analyses of Primate *HLA-F* genes—We identified primate *HLA-F* genes from gene and genome databases using a reciprocal BLAST strategy. Specifically, we used the human *HLA-F* gene as a query to BLAT search the Neanderthal, Denisovan, chimpanzee (CHIMP2.1.4), gorilla (gorGor3.1), orangutan (PPYG2), gibbon, (Nleu1.0), rhesus monkey (MMUL_1), hamadryas baboon (Pham_1.0), olive baboon (Panu_2.0), vervet monkey (ChlSab1.0), marmoset (C_jacchus3.2.1), Bolivian squirrel monkey (SalBol1.0), tarsier (tarSyr1), mouse lemur (micMur1), and galago (OtoGar3) genomes. *HLA-F* genes were not identified in the marmoset, Bolivian squirrel monkey, tarsier

(tarSyr1), mouse lemur, or galago genomes indicating it is specific to Old World monkeys. We used the default settings in MUSCLE (implemented in Genious 6.1.2) to align primate *HLA-F* genes and the suite of analyses methods implemented in DataMonkey to quantify the strength and direction of selection acting on primate *HLA-F* genes. We identified the best-fitting model of nucleotide substitution for our alignment using Datamonkey, then we used the PRIME method to test for evidence of positive selection involving changes in amino acid properties.

Biolayer Interferometry Measurements—All BLI measurements were performed using a Blitz instrument at room temperature (22°C). Biotinylated LIR1 protein was immobilized on streptavidin sensors until saturation. Dilutions of HLA-F, HLA-F OC and W62R HLA-F from 0.5 – 42 μM were made in HBS. A HBS-only trace was subtracted from HLA-F measurements. Equilibrium dissociation constants were determined by nonlinear regression with Prism software using a shared Bmax given comparable immobilization of ligands.

Production of Jurkat reporter cells—β_2m-deficient Jurkats were previously generated via Cas9-mediated deletion and subsequently transduced with KIRζ chimeric constructs via lentiviral gene transfer as described previously (Garcia-Beltran et al., 2016). KIRζ chimeric receptors for the inhibitory KIR2DL3ζ (Allele *KIR2DL3*001*) and KIR3DL2ζ (Allele *KIR3DL2*001*) contain the respective extracellular domain (ECD) and transmembrane domain (TMD) fused with the cytoplasmic tail of the human CD3ζ chain comprising the triple immune tyrosine activating motif (ITAM). KIR3DS1ζ (Allele *KIR3DS1*013*) and KIR2DS4ζ (Allele *KIR2DS4*001*) were designed by fusing the respective ECD with the TMD of the inhibitory KIR3DL1 and the cytoplasmic tail of the CD3ζ chain. Constructs were ordered from GeneArt and cloned into a lentiviral transfer vector containing an SFFV promoter and IRES-driven puromycin resistance (kindly provided by Thomas Pertel). Lentiviral supernatant was obtained via three-plasmid lipofectamine transfection of 293T cells with psPAX2, pHEFVSV-G and the transfer vector. Transduced cells were selected in culture media with Puromycin (Sigma-Aldrich) and sorted for KIR expressing $CD3^+$ cells via fluorescence-activated cell sorting. Cells were cultured in RPMI-1640 containing L-glutamine, supplemented with 20% FBS Superior and 1 μg/ml Puromycin. KIR expression was assessed by staining with the following antibodies: anti-KIR3DS1/L1, anti-KIR3DL2/L1, anti-KIR2DL2/3 and anti-KIR2DS4.

Jurkat Reporter Cell Assay—Streptavidin-coupled beads were coated with biotinylated KIR-antibodies (anti-KIR3DS1/L1 clone REA168, Miltenyi, anti-KIR2DS4 clone JJC11.6, Miltenyi, anti-KIR2DL3 clone REA147, Miltenyi, anti-KIR3DL1/L2 clone 5.133, Miltenyi), free biotin and biotinylated HLA-F monomers for 1 hour at 4°C while rotating. 1 μg of antibody per 0.1 mg of beads, and biotinylated HLA-F monomers were coated at 110 pmol per 0.1 mg beads. Negative control beads were saturated with free biotin. 2.5×10^4 KIR2DL3ζ, KIR2DS4ζ, KIR3DS1ζ, or KIR3DL2ζ-JRC were co-incubated with 5μl of coated beads diluted in 50 μl PBS or blank control without beads for 5 hours at 37°C. Subsequently, cells were stained with anti-CD3 and anti-CD69 antibodies, washed and fixed with PBS/4% paraformaldehyde. Flow cytometry data were acquired with a BD FACS Canto

II and analyzed using FlowJo software version 10.2. Percentages of bead binding cells and $CD69^+$ cells are shown with display of median and interquartile range after subtraction of background (blank control). Data is derived from three independent experiments.

PBMC tetramer staining—PBMCs were purified via ficoll-gradient from healthy volunteers and used immediately for tetramer staining. PBMCs were incubated with 600 nM tetramer in blocking buffer for 45 minutes at room temperature in the dark. Blocking buffer is composed of sterile PBS, 3% FBS, 10% human serum and .02% NaN_3. PBMCs were then washed and incubated with antibodies for 30 minutes on ice in the dark. PBMC wash buffer is composed of PBS, 3% FBS and .02% NaN_3. After additional washes, PBMCs were analyzed on a BD LSR Fortessa. Tetramer staining data was analyzed with FlowJo software. Compensation beads were used to set voltages and perform compensation while isotype control antibodies were used to set NKR^+ gates. Tetramer positive gates were drawn with T22 negative control tetramers at ~$1\%^+$. Graphs were made and statistical significance analysis was performed with Prism software.

Quantification and Statistical Analysis

Information on the statistical tests used can be found in the Results and Figure Legends. Statistical analysis was performed with Prism software. For PBMC tetramer staining statistical significance analysis (Figure 7B), we compared the percentages of tetramer positive cells between tetramer types via the nonparametric Friedman test with the repeated measures test to incorporate donor to donor variability (as in a pair-wise t-test) and Dunn's multiple comparison post-hoc test. * denotes significant (P value of 0.01–0.05).

Data and Software Availability

The structural data reported in this study were deposited in the Protein Data Bank under accession codes PDB: 5IUE (HLA-F structure) and PDB: 5KNM (HLA-F–LIR1 complex structure). The data on peptides eluted from WT and W62R HLA-F expressed in 293T cells can be found in the supplemental spreadsheet, Table S3.

Supplementary Material

Refer to Web version on PubMed Central for supplementary material.

Acknowledgments

We thank the staff of the Advanced Proton Source at GM/CA-CAT for assistance with X-ray beamlines; Michael Becker and Ruslan Sanishvili in particular for help and advice during data collection, the laboratory of Patrick C. Wilson for technical assistance with 293T expression, Cezary Ciszewski for advice and technical assistance with cellular assays, Qing Yu and Lingjun Li for help with preliminary HLA-F peptide analysis, Ivy Fitzgerald and Benjamin S. Glick for the gift of the pcDNA3.1-EGFP vector, Sean Crosson, Engin Özkan, and Adrienne Luoma for advice in data processing and refinement and Libby Guethlein, Paul Norman and Peter Parham for the LIR1 cDNA. We would also like to acknowledge all the contributions made to the field that we cannot cite due to length constraints. The authors declare no conflicts of interest.

This work was supported by the University of Chicago Molecular and Cellular Biology Training Grant (T32 GM007183) and NIH R01 AI073922 to E.J.A. A.H. was supported by the German Center for Infection Research (DZIF) through a MD/PhD Stipend and via the Clinician Scientist Program of the Faculty of Medicine, University Medical Centre Hamburg-Eppendorf, Hamburg, Germany.

References

Adams EJ, Luoma AM. The Adaptable Major Histocompatibility Complex (MHC) Fold: Structure and Function of Nonclassical and MHC Class I–Like Molecules. Annu Rev Immunol. 2013; 31:529–561. [PubMed: 23298204]

Adams PD, Afonine PV, Bunkóczi G, Chen VB, Davis IW, Echols N, Headd JJ, Hung LW, Kapral GJ, Grosse-Kunstleve RW, et al. PHENIX: a comprehensive Python-based system for macromolecular structure solution. Acta Crystallogr D Biol Crystallogr. 2010; 66:213–221. [PubMed: 20124702]

Aricescu AR, Lu W, Jones EY. A time- and cost-efficient system for high-level protein production in mammalian cells. Acta Crystallogr D Biol Crystallogr. 2006; 62:1243–1250. [PubMed: 17001101]

Bergseng E, Dørum S, Arntzen MØ, Nielsen M, Nygård S, Buus S, de Souza GA, Sollid LM. Different binding motifs of the celiac disease-associated HLA molecules DQ2.5, DQ2.2, and DQ7.5 revealed by relative quantitative proteomics of endogenous peptide repertoires. Immunogenetics. 2014; 67:73–84. [PubMed: 25502872]

Bjorkman PJ, Saper MA, Samraoui B, Bennett WS, Strominger JL, Wiley DC. Structure of the human class I histocompatibility antigen, HLA-A2. Nature. 1987; 329:506–512. [PubMed: 3309677]

Blum JS, Wearsch PA, Cresswell P. Pathways of Antigen Processing. Annu Rev Immunol. 2013; 31:443–473. [PubMed: 23298205]

Braud V, Jones EY, McMichael A. The human major histocompatibility complex class Ib molecule HLA-E binds signal sequence-derived peptides with primary anchor residues at positions 2 and 9. Eur J Immunol. 1997; 27:1164–1169. [PubMed: 9174606]

Braud VM, Allan DSJ, O'Callaghan CA, Söderström K, D'Andrea A, Ogg GS, Lazetic S, Young NT, Bell JI, Phillips JH, et al. HLA-E binds to natural killer cell receptors CD94/NKG2A, B and C. Nature. 1998; 391:795–799. [PubMed: 9486650]

Brown JH, Jardetzky TS, Gorga JC, Stern LJ, Urban RG, Strominger JL, Wiley DC. Three-dimensional structure of the human class II histocompatibility antigen HLA-DR1. Nature. 1993; 364:33–39. [PubMed: 8316295]

Burrows CK, Kosova G, Herman C, Patterson K, Hartmann KE, Edwards DRV, Stephenson MD, Lynch VJ, Ober C. Expression Quantitative Trait Locus Mapping Studies in Mid-secretory Phase Endometrial Cells Identifies HLA-F and TAP2 as Fecundability-Associated Genes. PLOS Genet. 2016; 12:e1005858. [PubMed: 27447835]

Carter AM, Enders AC, Pijnenborg R. The role of invasive trophoblast in implantation and placentation of primates. Philos Trans R Soc B Biol Sci. 2015; 370

Chapman TL, Heikema AP, Bjorkman PJ. The Inhibitory Receptor LIR-1 Uses a Common Binding Interaction to Recognize Class I MHC Molecules and the Viral Homolog UL18. Immunity. 1999; 11:603–613. [PubMed: 10591185]

Clements CS, Kjer-Nielsen L, Kostenko L, Hoare HL, Dunstone MA, Moses E, Freed K, Brooks AG, Rossjohn J, McCluskey J. Crystal structure of HLA-G: a nonclassical MHC class I molecule expressed at the fetal-maternal interface. Proc Natl Acad Sci U S A. 2005; 102:3360–3365. [PubMed: 15718280]

Coe CL, Lubach GR. Vital and Vulnerable Functions of the Primate Placenta Critical for Infant Health and Brain Development. Front Neuroendocrinol. 2014; 35:439–446. [PubMed: 24699357]

Colonna M, Navarro F, Bellón T, Llano M, García P, Samaridis J, Angman L, Cella M, López-Botet M. A Common Inhibitory Receptor for Major Histocompatibility Complex Class I Molecules on Human Lymphoid and Myelomonocytic Cells. J Exp Med. 1997; 186:1809–1818. [PubMed: 9382880]

Conant GC, Wagner GP, Stadler PF. Modeling amino acid substitution patterns in orthologous and paralogous genes. Mol Phylogenet Evol. 2007; 42:298–307. [PubMed: 16942891]

Fahnestock ML, Tamir I, Narhi L, Bjorkman PJ. Thermal stability comparison of purified empty and peptide-filled forms of a class I MHC molecule. Science. 1992; 258:1658–1662. [PubMed: 1360705]

Favier B, Lemaoult J, Lesport E, Carosella ED. ILT2/HLA-G interaction impairs NK-cell functions through the inhibition of the late but not the early events of the NK-cell activating synapse. FASEB J Off Publ Fed Am Soc Exp Biol. 2010; 24:689–699.

Ferreira LMR, Meissner TB, Tilburgs T, Strominger JL. HLA-G: At the Interface of Maternal–Fetal Tolerance. Trends Immunol. 2017

Fitzgerald I, Glick BS. Secretion of a foreign protein from budding yeasts is enhanced by cotranslational translocation and by suppression of vacuolar targeting. Microb Cell Factories. 2014; 13:125.

Garboczi DN, Hung DT, Wiley DC. HLA-A2-peptide complexes: refolding and crystallization of molecules expressed in Escherichia coli and complexed with single antigenic peptides. Proc Natl Acad Sci U S A. 1992; 89:3429–3433. [PubMed: 1565634]

Garcia-Beltran WF, Hölzemer A, Martrus G, Chung AW, Pacheco Y, Simoneau CR, Rucevic M, Lamothe-Molina PA, Pertel T, Kim TE, et al. Open conformers of HLA-F are high-affinity ligands of the activating NK-cell receptor KIR3DS1. Nat Immunol. 2016; 17:1067–1074. [PubMed: 27455421]

Geraghty DE, Wei XH, Orr HT, Koller BH. Human leukocyte antigen F (HLA-F). An expressed HLA gene composed of a class I coding sequence linked to a novel transcribed repetitive element. J Exp Med. 1990; 171:1–18. [PubMed: 1688605]

Godeau F, Luescher IF, Ojcius DM, Saucier C, Mottez E, Cabanie L, Kourilsky P. Purification and ligand binding of a soluble class I major histocompatibility complex molecule consisting of the first three domains of H-2Kd fused to beta 2-microglobulin expressed in the baculovirus-insect cell system. J Biol Chem. 1992; 267:24223–24229. [PubMed: 1447172]

Goodridge JP, Burian A, Lee N, Geraghty DE. HLA-F complex without peptide binds to MHC class I protein in the open conformer form. J Immunol. 2010; 184:6199–6208. [PubMed: 20483783]

Goodridge JP, Burian A, Lee N, Geraghty DE. HLA-F and MHC Class I Open Conformers Are Ligands for NK Cell Ig-like Receptors. J Immunol. 2013; 191:3553–3562. [PubMed: 24018270]

Hackmon R, Pinnaduwage L, Zhang J, Lye SJ, Geraghty DE, Dunk CE. Definitive class I human leukocyte antigen expression in gestational placentation: HLA-F, HLA-E, HLA-C, and HLA-G in extravillous trophoblast invasion on placentation, pregnancy, and parturition. Am J Reprod Immunol N Y N 1989. 2017

Ishitani A, Sageshima N, Lee N, Dorofeeva N, Hatake K, Marquardt H, Geraghty DE. Protein expression and peptide binding suggest unique and interacting functional roles for HLA-E, F, and G in maternal-placental immune recognition. J Immunol. 2003; 171:1376–1384. [PubMed: 12874228]

Jiang H, Canfield SM, Gallagher MP, Jiang HH, Jiang Y, Zheng Z, Chess L. HLA-E–restricted regulatory CD8+ T cells are involved in development and control of human autoimmune type 1 diabetes. J Clin Invest. 2010; 120:3641–3650. [PubMed: 20877010]

Körner C, Altfeld M. Role of KIR3DS1 in human diseases. Front Immunol. 2012; 3:326. [PubMed: 23125843]

Kraemer T, Celik AA, Huyton T, Kunze-Schumacher H, Blasczyk R, Bade-Döding C. HLA-E: Presentation of a Broader Peptide Repertoire Impacts the Cellular Immune Response—Implications on HSCT Outcome. Stem Cells Int. 2015; 2015

Lee N, Goodlett DR, Ishitani A, Marquardt H, Geraghty DE. HLA-E surface expression depends on binding of TAP-dependent peptides derived from certain HLA class I signal sequences. J Immunol Baltim Md 1950. 1998; 160:4951–4960.

Lepin EJ, Bastin JM, Allan DS, Roncador G, Braud VM, Mason DY, van der Merwe PA, McMichael AJ, Bell JI, Powis SH, et al. Functional characterization of HLA-F and binding of HLA-F tetramers to ILT2 and ILT4 receptors. Eur J Immunol. 2000; 30:3552–3561. [PubMed: 11169396]

Madden DR, Gorga JC, Strominger JL, Wiley DC. The three-dimensional structure of HLA-B27 at 2.1 Å resolution suggests a general mechanism for tight peptide binding to MHC. Cell. 1992; 70:1035–1048. [PubMed: 1525820]

McCoy AJ, Grosse-Kunstleve RW, Adams PD, Winn MD, Storoni LC, Read RJ. Phaser crystallographic software. J Appl Crystallogr. 2007; 40:658–674. [PubMed: 19461840]

McMurtrey C, Trolle T, Sansom T, Remesh SG, Kaever T, Bardet W, Jackson K, McLeod R, Sette A, Nielsen M, et al. Toxoplasma gondii peptide ligands open the gate of the HLA class I binding groove. eLife. 2016; 5:e12556. [PubMed: 26824387]

Morgan CS, Holton JM, Olafson BD, Bjorkman PJ, Mayo SL. Circular dichroism determination of class I MHC-peptide equilibrium dissociation constants. Protein Sci. 1997; 6:1771–1773. [PubMed: 9260291]

O'Callaghan CA, Bell JI. Structure and function of the human MHC class Ib molecules HLA-E, HLA-F and HLA-G. Immunol Rev. 1998; 163:129–138. [PubMed: 9700506]

O'Callaghan CA, Tormo J, Willcox BE, Braud VM, Jakobsen BK, Stuart DI, McMichael AJ, Bell JI, Jones EY. Structural features impose tight peptide binding specificity in the nonclassical MHC molecule HLA-E. Mol Cell. 1998; 1:531–541. [PubMed: 9660937]

O'Connor GM, McVicar D. The yin-yang of KIR3DL1/S1: molecular mechanisms and cellular function. Crit Rev Immunol. 2013; 33:203–218. [PubMed: 23756244]

O'Connor GM, Vivian JP, Gostick E, Pymm P, Lafont BAP, Price DA, Rossjohn J, Brooks AG, McVicar DW. Peptide-Dependent Recognition of HLA-B*57:01 by KIR3DS1. J Virol. 2015; 89:5213–5221. [PubMed: 25740999]

Raran-Kurussi S, Keefe K, Waugh DS. Positional effects of fusion partners on the yield and solubility of MBP fusion proteins. Protein Expr Purif. 2015; 110:159–164. [PubMed: 25782741]

Romagnani C, Pietra G, Falco M, Millo E, Mazzarino P, Biassoni R, Moretta A, Moretta L, Mingari MC. Identification of HLA-E-specific alloreactive T lymphocytes: A cell subset that undergoes preferential expansion in mixed lymphocyte culture and displays a broad cytolytic activity against allogeneic cells. Proc Natl Acad Sci. 2002; 99:11328–11333. [PubMed: 12167676]

Saper MA, Bjorkman PJ, Wiley DC. Refined structure of the human histocompatibility antigen HLA-A2 at 2.6 Å resolution. J Mol Biol. 1991; 219:277–319. [PubMed: 2038058]

Shiroishi M, Kuroki K, Rasubala L, Tsumoto K, Kumagai I, Kurimoto E, Kato K, Kohda D, Maenaka K. Structural basis for recognition of the nonclassical MHC molecule HLA-G by the leukocyte Ig-like receptor B2 (LILRB2/LIR2/ILT4/CD85d). Proc Natl Acad Sci. 2006; 103:16412–16417. [PubMed: 17056715]

Shobu T, Sageshima N, Tokui H, Omura M, Saito K, Nagatsuka Y, Nakanishi M, Hayashi Y, Hatake K, Ishitani A. The surface expression of HLA-F on decidual trophoblasts increases from mid to term gestation. J Reprod Immunol. 2006; 72:18–32. [PubMed: 16806485]

Smith K, Garman L, Wrammert J, Zheng NY, Capra JD, Ahmed R, Wilson PC. Rapid generation of fully human monoclonal antibodies specific to a vaccinating antigen. Nat Protoc. 2009; 4:372–384. [PubMed: 19247287]

Song S, Miranda CJ, Braun L, Meyer K, Frakes AE, Ferraiuolo L, Likhite S, Bevan AK, Foust KD, McConnell MJ, et al. Major histocompatibility complex class I molecules protect motor neurons from astrocyte-induced toxicity in amyotrophic lateral sclerosis. Nat Med. 2016; 22:397–403. [PubMed: 26928464]

Strong RK, Holmes MA, Li P, Braun L, Lee N, Geraghty DE. HLA-E Allelic Variants CORRELATING DIFFERENTIAL EXPRESSION, PEPTIDE AFFINITIES, CRYSTAL STRUCTURES, AND THERMAL STABILITIES. J Biol Chem. 2003; 278:5082–5090. [PubMed: 12411439]

Trolle T, McMurtrey CP, Sidney J, Bardet W, Osborn SC, Kaever T, Sette A, Hildebrand WH, Nielsen M, Peters B. The Length Distribution of Class I-Restricted T Cell Epitopes Is Determined by Both Peptide Supply and MHC Allele-Specific Binding Preference. J Immunol Baltim Md 1950. 2016; 196:1480–1487.

Wainwright SD, Biro PA, Holmes CH. HLA-F is a predominantly empty, intracellular, TAP-associated MHC class Ib protein with a restricted expression pattern. J Immunol Baltim Md 1950. 2000; 164:319–328.

Wang CR, Castaño AR, Peterson PA, Slaughter C, Lindahl KF, Deisenhofer J. Nonclassical binding of formylated peptide in crystal structure of the MHC class lb molecule H2-M3. Cell. 1995; 82:655–664. [PubMed: 7664344]

Willcox BE, Thomas LM, Bjorkman PJ. Crystal structure of HLA-A2 bound to LIR-1, a host and viral major histocompatibility complex receptor. Nat Immunol. 2003; 4:913–919. [PubMed: 12897781]

Winn MD, Ballard CC, Cowtan KD, Dodson EJ, Emsley P, Evans PR, Keegan RM, Krissinel EB, Leslie AGW, McCoy A, et al. Overview of the CCP4 suite and current developments. Acta Crystallogr D Biol Crystallogr. 2011; 67:235–242. [PubMed: 21460441]

Winter G. xia2: an expert system for macromolecular crystallography data reduction. J Appl Crystallogr. 2010; 43:186–190.

Yaciuk JC, Skaley M, Bardet W, Schafer F, Mojsilovic D, Cate S, Stewart CJ, McMurtrey C, Jackson KW, Buchli R, et al. Direct Interrogation of Viral Peptides Presented by the Class I HLA of HIV-Infected T Cells. J Virol. 2014; 88:12992–13004. [PubMed: 25165114]

Yang Z, Bjorkman PJ. Structure of UL18, a peptide-binding viral MHC mimic, bound to a host inhibitory receptor. Proc Natl Acad Sci. 2008; 105:10095–10100. [PubMed: 18632577]

Highlights

- The crystal structure of HLA-F reveals a unique mode of peptide presentation
- LIR1 recognizes β_2m-HLA-F via a docking strategy that precludes HLA-F OC recognition
- Peptide-bound HLA-F and empty HLA-F OC are recognized by distinct NKRs
- Peptide binding increases the proportion of leukocytes that stain with HLA-F tetramer

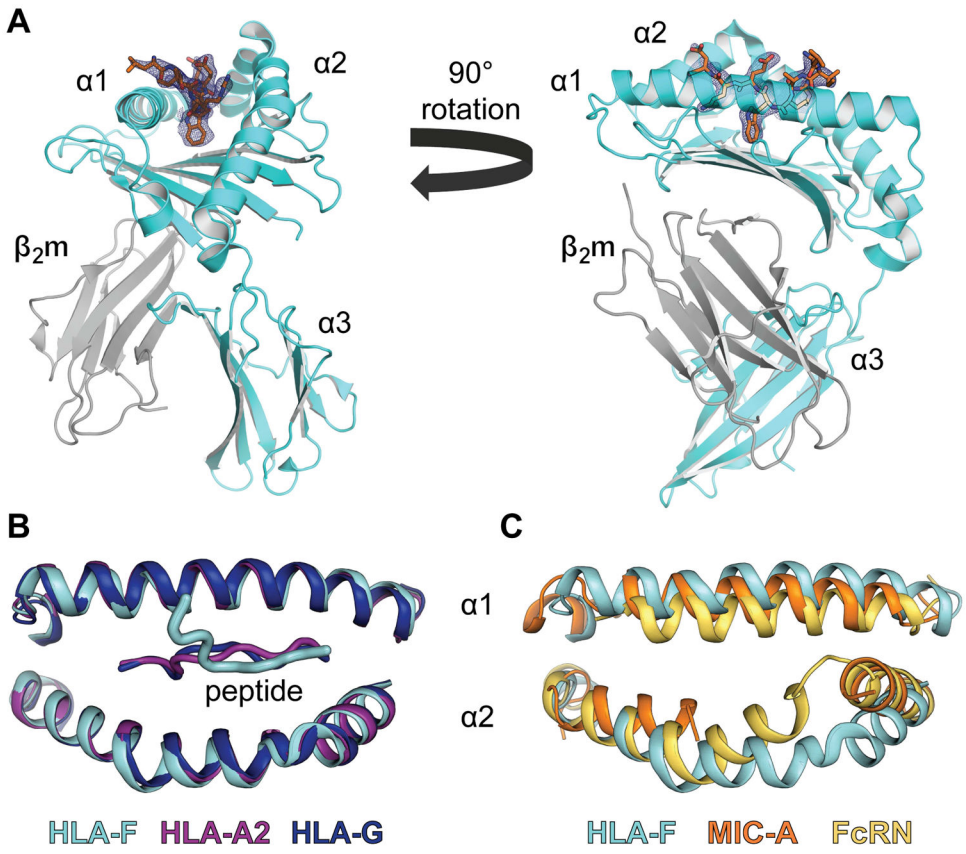

Figure 1. The crystal structure of HLA-F reveals a conserved MHC scaffold with a peptide-presenting groove

Overview of the crystal structure of the HLA-F-antigen complex. **(A)** Ribbon diagrams of the extracellular portion of HLA-F in complex with β_2m. The α1, α2 and α3 domains of HLA-F are in cyan; β_2m is in grey; and peptide is in orange with side-chain oxygen and nitrogen in red and blue, respectively. Around the peptide, a $2F_o$-F_c electron density map (blue mesh) contoured at 1σ is displayed showing the electron density seen in the groove that is attributed to bound peptide. **(B)** Overlay of the α1 and α2 helices of the antigen-binding cleft of HLA-F with the peptide-presenting MHC-I molecules, HLA-A2 (purple, PDB ID 1HHI) and HLA-G (dark blue, PDB ID 1YDP) with bound peptides shown as tubes. **(C)** Overlay of the α1 and α2 helices of HLA-F with the non-peptide-presenting MHC-like molecules, MIC-A (orange, PDB ID 1B3J) and FcRN (yellow, PDB ID 1EXU). Please also see Table S1 and Figure S1.

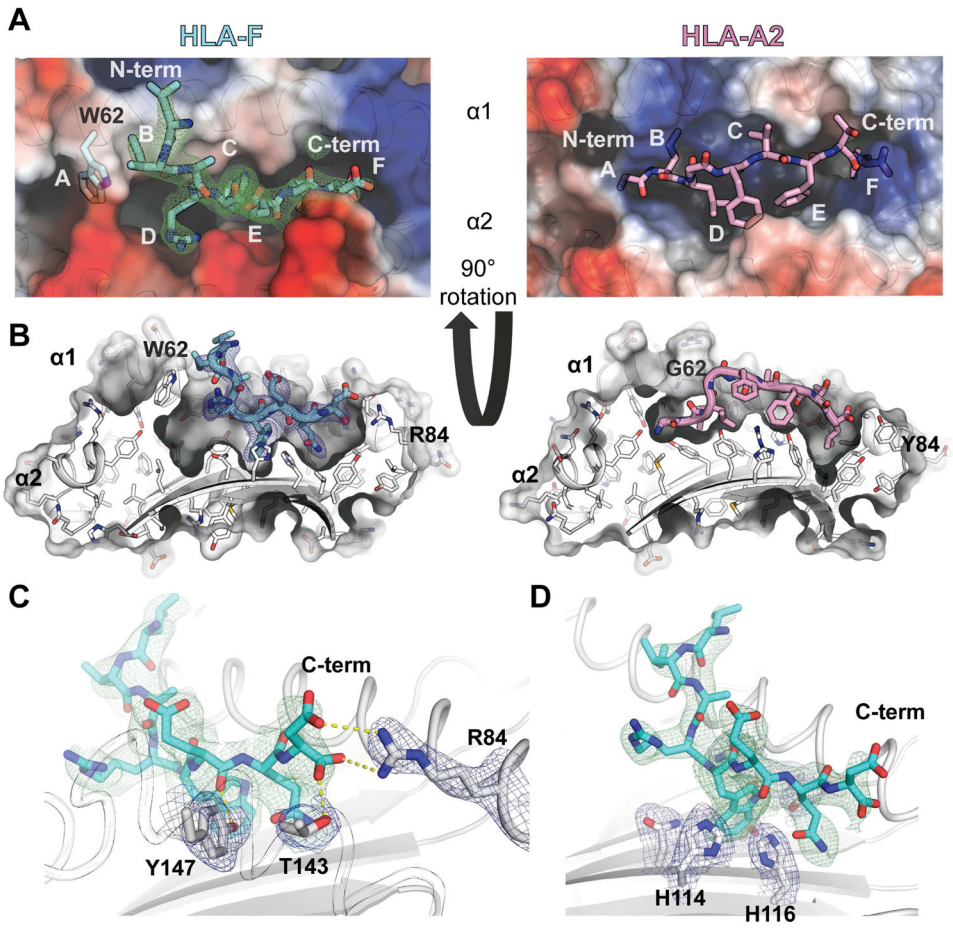

Figure 2. The unique molecular landscape of the HLA-F groove evolved to present peptides via an unconventional mechanism

(A) A comparison of the electrostatic surfaces of the peptide-binding clefts of HLA-F (left) and HLA-A2 (right) from a top-down perspective. The MHC-I binding pockets that accommodate peptide side-chains within the groove are labeled A–F. **(B)** A comparison of the molecular landscapes of the HLA-F and HLA-A2 grooves from a cut-away, side perspective. The HLA-F peptide (cyan) has an unanchored N-terminus, which snakes up and out of the groove while the HLA-A2 peptide (pink) is anchored at both termini (canonical MHC-I peptide presentation is demonstrated by HLA-A2). Electron density for the HLA-F peptide is shown via a $2F_o$-F_c electron density map (blue or green mesh) contoured at 1σ. **(C)** A close-up representation of the HLA-F groove displaying the C-terminus of bound peptide anchored via salt-bridges and hydrogen bonds (dashed yellow lines). **(D)** An enlarged view of the His-His motif and other residues at the floor of the HLA-F groove that form the C pocket. Please also see Figure S2 and Table S2.

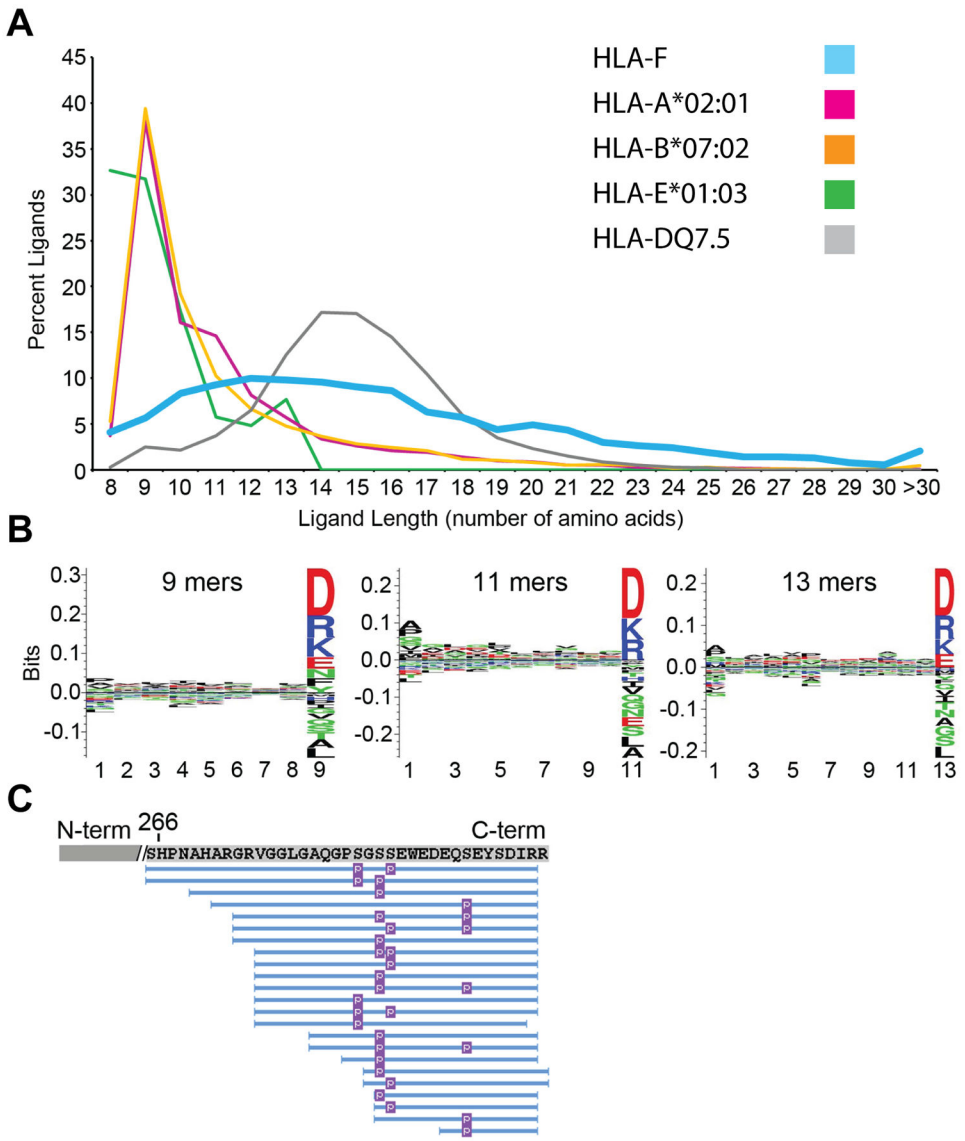

Figure 3. HLA-F presents endogenous peptides of a length distribution reminiscent of MHC-II

(A) Length distribution of HLA-F peptides (blue) compared to published length distributions of other MHC-I: HLA-A*02:01 (magenta) (Trolle et al., 2016), HLA-B*07:02 (orange) (Trolle et al., 2016), HLA-E*01:03 (green) (Kraemer et al., 2015), HLA-DQ7.5 (grey) (Bergseng et al., 2014). **(B)** Observed motif of HLA-F peptides grouped by representative lengths: 9-mers (left), 11-mers (middle), 13-mers (right). **(C)** List of stanniocalcin 2-originating phosphorylated peptides eluted from HLA-F aligned to the C-terminal sequence of stanniocalcin 2. Please also see Table S3 and Figure S3.

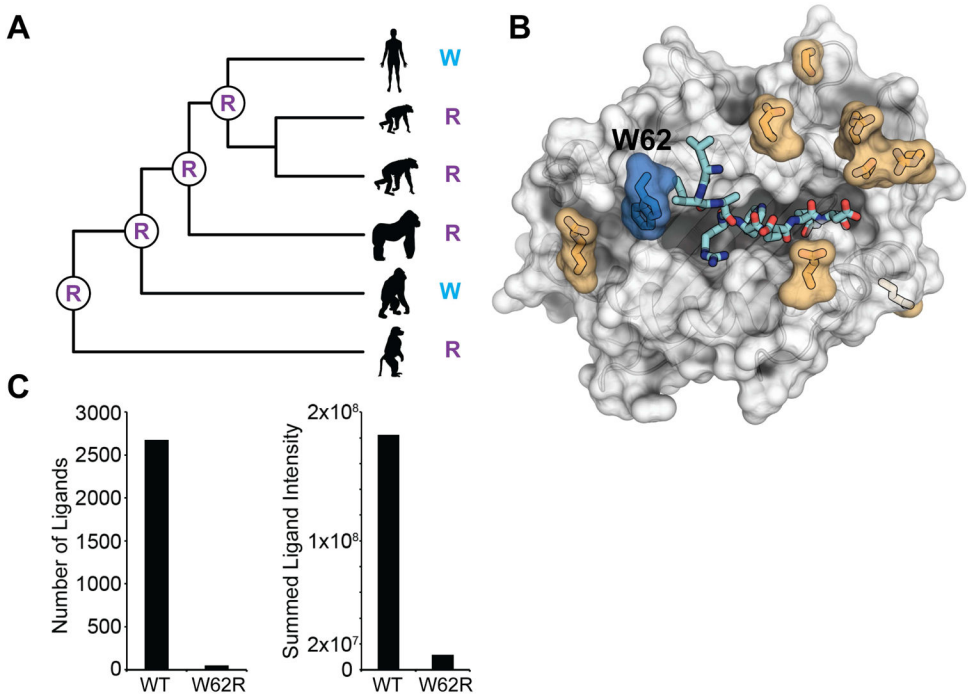

Figure 4. The R62W substitution converted HLA-F into a peptide-presenting molecule

(A) An evolutionary tree depicting the convergent substitution of arginine62 (R) to tryptophan (W) in the human and orangutan lineages. **(B)** A top-down perspective of the human HLA-F groove in surface representation with residues that vary in primates shown in orange as sticks and W62 shown in blue. The R62W substitution is the only nonconservative amino acid change between the groove of human and chimpanzee HLA-F. **(C)** Number of unique eluted peptides from WT and W62R HLA-F (left). Summed MS1 extracted ion area-underneath-the-curve intensity for all the eluted peptides from WT and W62R HLA-F (right). Intensities are normalized to the total quantity of HLA-F used for each elution experiment. Please also see Table S4 and Figure S4.

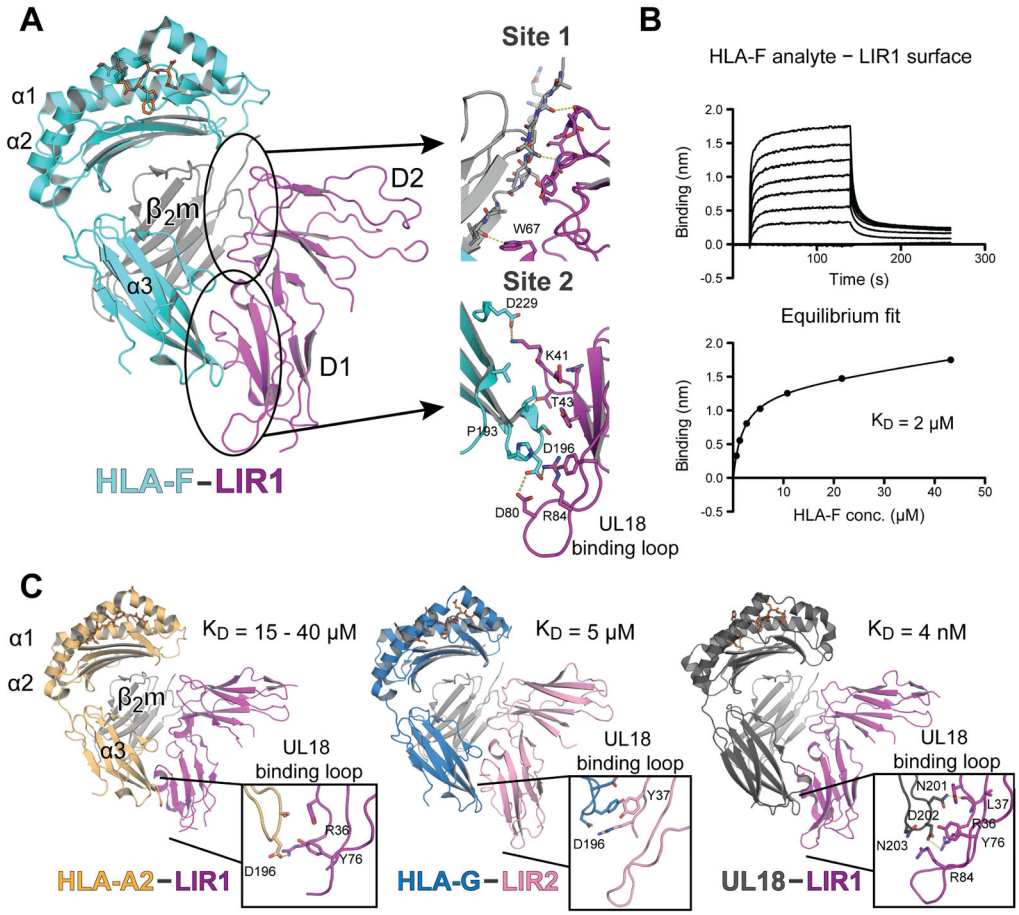

Figure 5. Recognition of β_2m-HLA-F by LIR1 is mediated via a conserved docking strategy that precludes OC binding and is reminiscent of UL18 recognition

(A) Ribbon diagram of the β_2m-HLA-F-LIR1 D1–D2 structure with HLA-F shown in cyan, β_2m in grey and LIR1 D1–D2 in magenta. Enlarged views of site 1 and site 2 recognition interfaces are shown on the right with important interaction residues shown as sticks and hydrogen bonds shown as yellow dashes. **(B)** Association and dissociation binding curves of β_2m-HLA-F and LIR1 measured by BLI (top). Scatchard plot showing the equilibrium binding constant (K_D) for β_2m-HLA-F and LIR1 (bottom). **(C)** Cartoonrepresentations of the complex crystal structures of HLA-A2-LIR1 D1-D2, HLA-G-LIR2 D1–D2 and UL18-LIR1 D1–D2 (PDB IDs 1P7Q, 2DYP and 3D2U, respectively) showing an overall conserved docking orientation for LIR recognition of the MHC-I scaffold. Enlarged insets show the orientation and differential usage of the UL18 binding loop of LIR1 to recognize various MHC α3 domains. Please also see Figure S4, Figure S5 and Table S5.

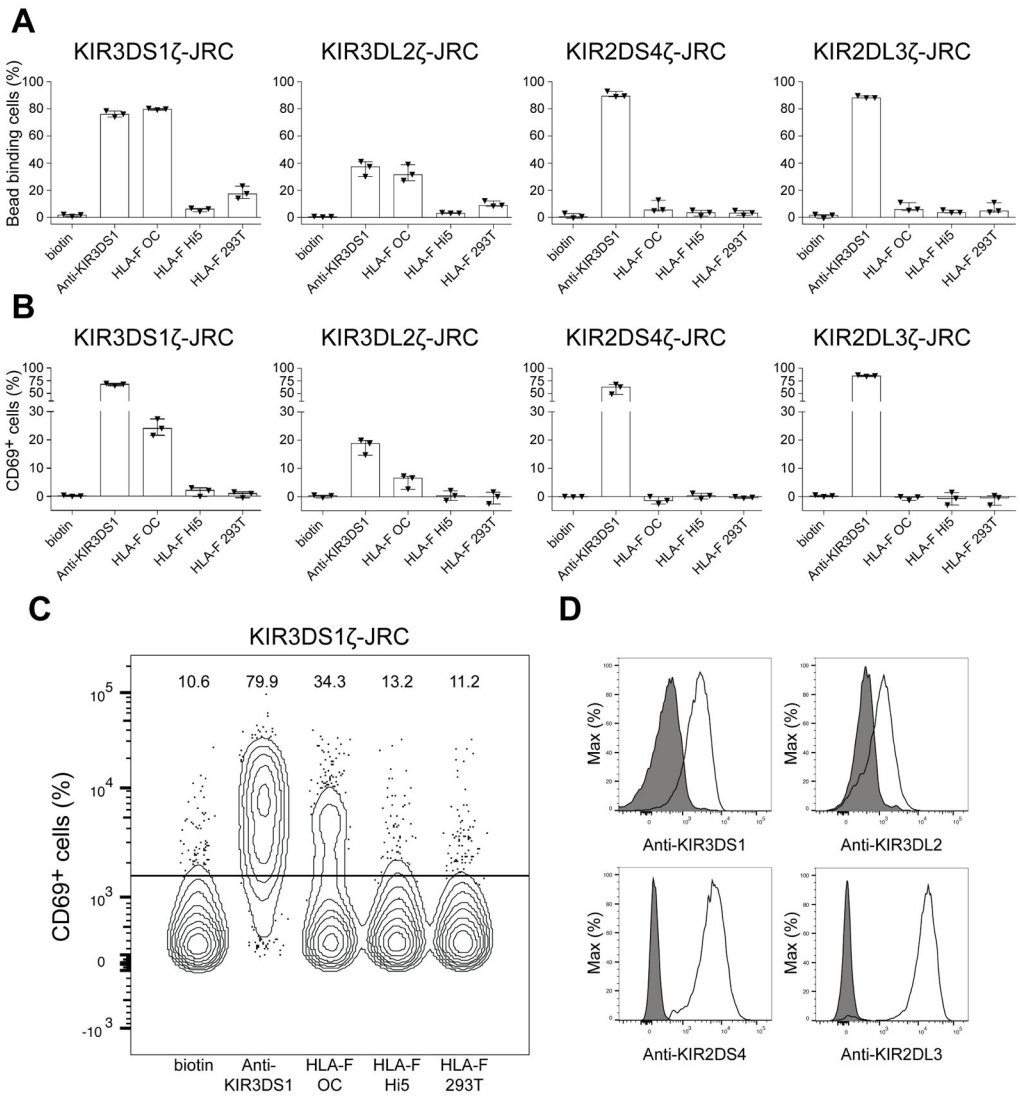

Figure 6. Peptide binding prevents HLA-F recognition and triggering of KIR3D

(A) Binding to Jurkat reporter cells (JRC) transduced with KIRζ is reported as percentage of bead-bound cells after co-incubation with beads coated with HLA-F OC or peptide-bound forms of HLA-F (HLA-F Hi5, HLA-F 293T). Biotin-coated beads or Anti-KIR antibody-coated beads were used as negative or positive controls, respectively. KIR2DL3ζ-JRC served as a negative control cell line for HLA-F binding. **(B)** Reporter activity (measured as percentages of $CD69^+$ cells) of KIRζ-JRC after co-incubation with beads coated as in (A). Data in (A) and (B) are displayed as percentages derived from three independent experiments with median and interquartile range after background subtraction. **(C)** Contour flow plot displaying the percentages of $CD69^+$ KIR3DS1ζ-JRC after co-incubation with beads coated as in (A). **(D)** Histograms depicting KIRζ expression levels of JRC compared to untransduced parent Jurkat cell line (shaded) following staining with indicated antibodies.

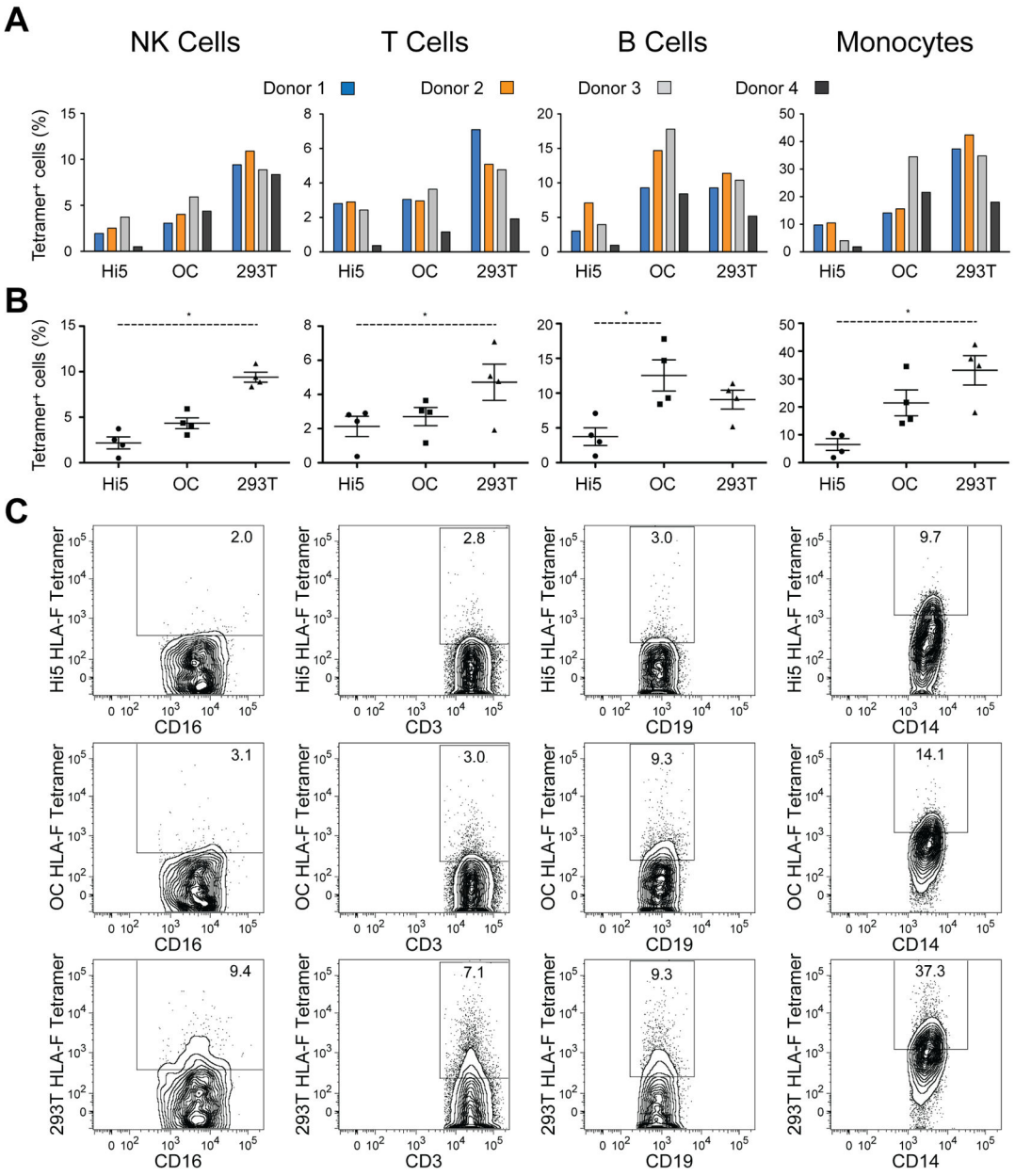

Figure 7. HLA-F tetramers bound with human peptides stain a greater percentage of NK cells, T cells and monocytes

(A) Summary data for HLA-F tetramer staining of PBMCs isolated from 4 normal donors. **(B)** For statistical analysis, we compared the percentages of tetramer$^+$ cells (mean and the standard error of the mean displayed) between tetramer types via a Friedman test; * denotes significant (P value of 0.01–0.05). **(C)** Contour flow plots of PBMC staining with HLA-F tetramers produced in Hi5 insect cells, as refolded open conformers (OC) or in 293T cells. Gating shows the percentages of CD16$^+$ NK cells, CD3$^+$ T cells, CD19$^+$ B cells or CD14$^+$ monocytes that are HLA-F tetramer$^+$. Gates were drawn based on T22 negative control tetramer staining. Please also see Figure S6.